

Correlated power time series of individual wind turbines: A data driven model approach

Cite as: J. Renewable Sustainable Energy **12**, 023301 (2020); <https://doi.org/10.1063/1.5139039>
Submitted: 18 November 2019 • Accepted: 06 February 2020 • Published Online: 06 March 2020

 Tobias Braun, Matthias Waechter, Joachim Peinke, et al.



View Online



Export Citation



CrossMark

ARTICLES YOU MAY BE INTERESTED IN

[Energy, atmospheric physics, and climate: On the scientific role of the Journal of Renewable and Sustainable Energy](#)

Journal of Renewable and Sustainable Energy **12**, 010401 (2020); <https://doi.org/10.1063/5.0004149>

[Data-driven modeling of the wake behind a wind turbine array](#)

Journal of Renewable and Sustainable Energy **12**, 033304 (2020); <https://doi.org/10.1063/5.0004393>

[Correlation analysis for wind speed and failure rate of wind turbines using time series approach](#)

Journal of Renewable and Sustainable Energy **4**, 032301 (2012); <https://doi.org/10.1063/1.4730597>

Scilight

Summaries of the latest breakthroughs
in the **physical sciences**



Correlated power time series of individual wind turbines: A data driven model approach

Cite as: J. Renewable Sustainable Energy **12**, 023301 (2020); doi: 10.1063/1.5139039

Submitted: 18 November 2019 · Accepted: 6 February 2020 ·

Published Online: 6 March 2020



View Online



Export Citation



CrossMark

Tobias Braun,^{1,a)}  Matthias Waechter,² Joachim Peinke,² and Thomas Cuhr¹

AFFILIATIONS

¹Faculty of Physics, University of Duisburg-Essen, Lotharstrasse 1, 47057 Duisburg, Germany

²ForWind and Institute of Physics, Carl-von-Ossietzky University Oldenburg, K pkersweg 70, 26129 Oldenburg, Germany

^{a)}Present address: Potsdam Institute for Climate Impact Research, PIK, Potsdam, Germany.

Author to whom correspondence should be addressed: tobraun@pik-potsdam.de

ABSTRACT

Wind farms can be regarded as complex systems that are, on the one hand, coupled to the nonlinear, stochastic characteristics of weather and, on the other hand, strongly influenced by supervisory control mechanisms. One crucial problem in this context today is the predictability of wind energy as an intermittent renewable resource with additional non-stationary nature. In this context, we analyze the power time series measured in an offshore wind farm for a total period of one year with a time resolution of 10 min. Applying detrended fluctuation analysis, we characterize the autocorrelation of power time series and find a Hurst exponent in the persistent regime with cross-over behavior. To enrich the modeling perspective of complex large wind energy systems, we develop a stochastic reduced-form model of power time series. The observed transitions between two dominating power generation phases are reflected by a bistable deterministic component, while correlated stochastic fluctuations account for the identified persistence. The model succeeds to qualitatively reproduce several empirical characteristics such as the autocorrelation function and the bimodal probability density function.

  2020 Author(s). All article content, except where otherwise noted, is licensed under a Creative Commons Attribution (CC BY) license (<http://creativecommons.org/licenses/by/4.0/>). <https://doi.org/10.1063/1.5139039>

I. INTRODUCTION

In the context of anthropogenic climate changes, the challenge of reducing carbon emissions is of central importance. Renewable sources of energy are considered to be one of the most promising solutions in the electricity sector to cover an increasing energy demand without exacerbating high carbon emissions coupled to it. Wind energy in particular appears to be one of the most strongly increasing sources of renewable energy^{1,2} but demands an extraordinary adaption of grids and related power systems due to its intermittent nature.^{3,4} It consequently raises the need for a profound understanding of this intermittency and the opportunity to perform extensive studies on the reliability of power systems by suitable models. Such models can only be calibrated with respect to empirical data, while different approaches are required to reflect features on multiple spatial and temporal scales.^{5,6} Moreover, they can be used to study the impact of certain well known statistical characteristics on the resulting dynamics. This provides wind farm (WF) controllers with a rich set of tools to analyze variable scenarios taking influences into account, which are known to be of importance.

In this work, we focus on the dynamics of single wind turbine (WT) power generation in an offshore wind farm. While especially

power generation of aggregated wind farms or even complexes of several wind farms has received considerable attention, the challenge of intermittent and stochastic characteristics is particularly high on the scale of single turbines.⁷ Still, it does not vanish for larger units such as wind farms or national wide wind power generation.⁸ How generated power fluctuations from geographically separated wind farms are dampened when aggregated^{9,10} is of crucial importance for large scale grid stability.^{11,12}

Our perspective on this problem is to study the autocorrelation of power time series as an indicator of their intermittent and nonstationary nature in the first step. In most modeling approaches, information on the complex temporal evolution of variations is included, and hence, autocorrelation is of great general importance. Nonstationarity is another feature that is frequently encountered dealing with complex systems.¹³ We address this within the analysis of power output correlations using the popular method of detrended fluctuation analysis (DFA).¹⁴ It can deal with polynomial nonstationarities in a generalized fashion. The fluctuations around these polynomial trends are subject to the correlation analysis, which yields a Hurst exponent as an indicator for the strength and nature of the autocorrelation.

The idea that power time series should exhibit scaling behavior is based on the finding that the underlying wind speed dynamics are governed by atmospheric turbulence.¹⁵ The traditional tool to capture this aspect is the power spectrum obtained by Fourier analysis.¹⁶ Several studies have examined the power spectral density for both wind speed^{17,18} and power time series,^{19,20} also uncovering how aggregation on different spatial scales impacts power fluctuations.^{10,21} Other classical methods range from structure functions to estimators for the Hurst exponent based on the scale dependent variance calculation on the respective time series.²² Still, these methods do not take the above-mentioned nonstationarity into account. To this extent, several works study the autocorrelation of wind speed time series $u(t)$ applying DFA and multifractal DFA (MFDFA) and conclude that it behaves persistent with a multifractal dependence.^{23–25} While most research in this context focuses on local wind speed measurements of single sites, some studies reveal the multifractality of wind speed on a larger spatial scale, for instance,²⁶ incorporating wind speed data spatially distributed all over Switzerland and finding the multifractal dependence of persistence for the cooperative behavior in the context of monitoring systems. Similar research for power time series appears more limited. The authors of Refs. 27 and 28 revealed a high degree of multifractality for both wind speed and power time series of an aggregated wind farm and joined both in a description via generalized correlation functions. Furthermore, aggregated power output of wind farms is known to show complex correlations in terms of persistence and multifractality. The authors in Ref. 29 uncovered the multifractality for the power time series of an aggregated wind farm in South Australia with data on a similar timescale. They classify power time series in the persistent regime, especially on short timescales of several minutes. Yet, to the best of our knowledge, no research has employed DFA or multifractal methods focusing on single WT's power output.

After we have obtained a better understanding of autocorrelations, we put forward a model based on these theoretical insights and an important feature of the empirical probability density function (PDF) of power output. A broad range of approaches is considered for wind power generation models in the respective literature. A general distinction of models can be based on whether power is directly or indirectly modeled, e.g., by mapping certain variables such as measured wind speed on power via a distinct transformation. Our work contributes to direct power modeling of time series for single WTs. Most models aim at finding a precise point forecast of time series for a certain timescale and horizon.³⁰ In contrast to this, effort is put into modeling different properties related to power output such as the power curve,^{31,32} wind power ramps,³³ or power density estimates.³⁴ Models also vary in terms of the timescale³⁵ that ranges from the ultra-short-term (ms – s)³⁶ to long-term forecasts (months).³⁷

The model proposed in this work aims at modeling short-term power time series without the objective to give precise point forecasts. Instead, we aim at deepening the systemic understanding of a WT due to its stochastic nature on the one hand and the impact of control mechanisms (e.g., curtailment) on the other hand. Following this motivation, the model is based on a single nonlinear stochastic differential equation (SDE) that is split into two components in a Langevin fashion. Since WTs are directly coupled to the complex atmospheric dynamics of wind, it is paramount to incorporate a stochastic component that allows for a certain degree of complex diffusive behavior. A sufficient approach to include such complex diffusive dynamics

without a loss of simple applicability is given by fractional Gaussian noise (FGN).³⁸ Time series generated as FGN entail a certain degree of correlation and yield fractional Brownian motion (FBM) when cumulated. Thus, we are able to reflect on the results from the correlation analysis from a model perspective. The second component of our model takes the impact of control mechanisms on power output into account. We address this feature in two steps. A deterministic component in the differential equation accounts for the characteristic shape of the PDF as the first mechanism to focus the power values around the respective fixed points. The second step incorporates control mechanisms such as curtailing in a simplified numerical fashion. Finally, we include a simple first approach to account for a time dependent seasonal drive of power output as well. By constructing our model in such a way, its easily distinguishable components and parameters give a way to a better understanding of how certain theoretical features affect power time series qualitatively, such as the degree of autocorrelation. It further yields the opportunity to test parametrized scenarios and may be used in large power network simulations based on simplified models of single wind turbine dynamics.

This paper is organized as follows: we present the dataset and perform a cleansing procedure on it in Sec. II such that we can get the first impression of its fundamental characteristics afterwards. In Sec. III, we identify the autocorrelation of power time series via the traditional autocorrelation function and the method of DFA. The stochastic model we introduce in Sec. IV is based on these empirical findings and will enlarge upon our understanding of how varying autocorrelations have an impact on fundamental statistical features by comparison with the data. When we present the results, we will find a sufficient agreement between the empirical and modeled features. We summarize our results in Sec. V.

II. DATA TREATMENT AND CHARACTERISTIC FEATURES

We briefly introduce the dataset in Sec. II A. The data cleansing procedure described in Sec. II B is important to focus only on a reasonable subset of the empirical data.³⁹ Finally, we get a first glance of the most substantial characteristic features of the wind farm data in Sec. II C.

A. Dataset

The dataset we analyze comprises time series of 30 WTs located at the German offshore wind farm RIFFGAT. Several observables are measured via a SCADA (Supervisory Control and Data Acquisition) system; however, we will focus only on the active power output of the WTs. The respective time series cover a total period of one year between 01/03/2014 and 28/02/2015. All analysis is carried out on ten minute average values calculated from data points measured with 1 Hz frequency. Thus, the timestamp precision is limited to ten minutes, and we obtain 52 560 values in total.

B. Data cleansing

In the following, we briefly present the applied data cleansing procedure. We detect outliers and ensure that we only consider a reasonable subset of the initially measured data. Every data value we consider to be erroneous will be set to NA (not available) and is not included in any upcoming analysis. In the first step, we ensure that

there are no redundant timestamps in any time series and look for consecutive identical values. Since one ten minute average value is based on 600 measured values, it can be rated as a highly unlikely case that two consecutive 10-min averages are identical with a five digit precision in the data. This could only be conceivable if, e.g., constant rated power is generated for ten minutes without any variation. To rule out this case, we also took the maximum and minimum values for the respective ten minute intervals into account.

Apart from the ten minute average values, we inspect the respective standard deviations. Any data value with a vanishing ten minute standard deviation is set to NA. In the last step, we analyze if there are unreasonable changes of consecutive power values, which we will call power increments. We consider each power increment to be unreasonably high (regardless of its direction) if it meets both the following criteria: the power increment $\Xi_+ = (P(t+1) - P(t))/P_+$ relative to the so-called rated power output P_+ of the WT is higher than a certain threshold Ξ_0 and the respective minimum power P_{\min} in a ten minute time interval is higher than the maximum power P_{\max} in the previous time interval by a certain factor q : $P_{\min} > qP_{\max}$, which yields unphysical data. We choose the threshold value Ξ_0 and the factor q in a way that limits extreme power increments to a typical value found in the respective literature.⁴⁰ This yields $\Xi_0 = 0.67$ and $q = 0.99$. The higher these values are chosen, the more the unphysical ramps are still kept in the data, which results in a higher number of strong jumps between low and high power generation. If we apply a too strict choice, some of the true strong ramps that resemble intermittent fluctuations are spuriously eliminated, also biasing results for temporal correlations. After applying the stated cleansing steps, we obtain 9.58% of NA values in the data. We will only consider pairs of values containing no NA value in every calculation of correlations between time series.

C. Bimodality and power increments

To achieve a sufficient understanding of wind power data, some basic facts about the conversion of wind speed u into active power output P and the control of WTs have to be outlined.^{41,42} Although an increase in wind speed obviously leads to a higher gain of generated power in general, WTs only run within a certain operating range. This limitation is due to the finite performance of power generators. In fact, the operation of WTs is limited by a lower cut-in value u_- and an upper cut-off value u_+ of wind speed u . Below u_- , there is simply not enough wind energy for an economic use of the turbine so that $P = P_- (= 0 \text{ kW})$. When u exceeds u_+ , power is controlled to remain constant at the rated power output $P = P_+ (= 3600 \text{ kW})$. For even higher wind speeds, it becomes essential to avoid mechanical damage, and the WTs are turned down by a continuous adjustment of the rotor blades. Within $u_- \leq u \leq u_+$, the generated power of an ideal WT increases proportionally to u^3 . For this work, the most important conclusion to draw from these control mechanisms is that power time series have to be at least in parts artificially flattened. We expect power values to be constant at $P = P_-$ or $P = P_+$ for certain time periods.

This manifests itself in Fig. 1(a) as a striking bimodal pattern in the five displayed time series and a striking bimodality of the empirical PDF in Fig. 1(b), visualized as a histogram. Most power values are concentrated around zero power generation P_- and active power output P_+ . In fact, the intervals $50 \text{ kW} < P < 200 \text{ kW}$ and $3550 \text{ kW} < P < 3800 \text{ kW}$ around the two peaks sum up to 41.62% of all values. This feature also governs the dynamics observed from the time series

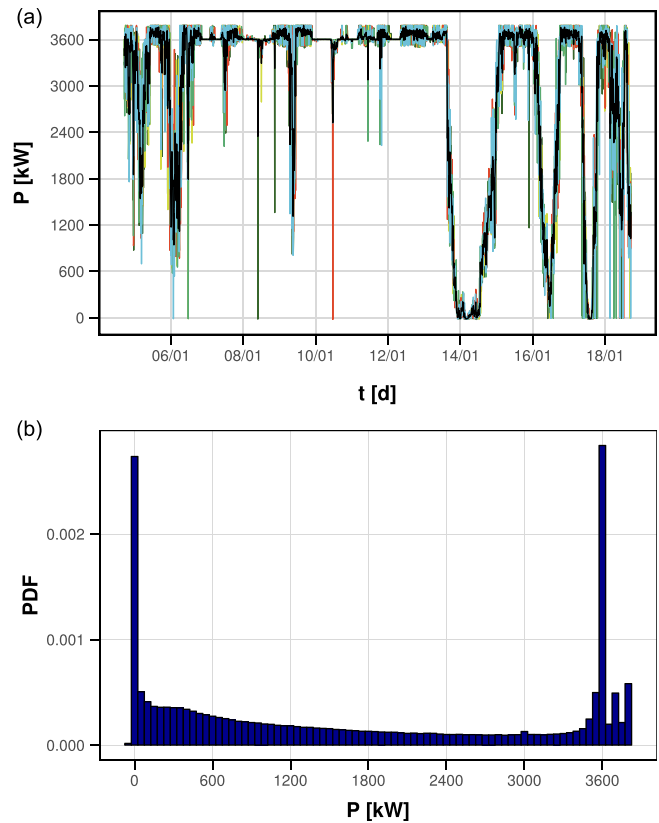


FIG. 1. Exemplary power time series and average power output (black) covering two weeks. The respective PDF plotted as a histogram is shown for all WTs covering the entire time period.

and is observed in several different works.^{43–45} Nevertheless, other analyses^{46,47} also show unimodal distributions around P_- or flatter, less concentrated distributions. While the first observation is related to the different efficiencies of WTs, the latter is mostly found for the aggregated power of several wind farms where WTs with different rated power outputs are combined. Despite this bimodal shape of the PDF, also values exceeding the rated power can be observed. Finally, strong downward ramps to zero power output can be observed for some of the WTs.

We will characterize such power ramps by the increments $\Xi_k(t) = P_k(t + \Delta t) - P_k(t)$, which are a fundamental property for the understanding and management of wind farms. We define them as the standardized, dimensionless differences

$$\tilde{\Xi}_k(t) = \frac{\Xi_k(t) - \frac{1}{T} \sum_{t=1}^T \Xi_k(t)}{\sqrt{\frac{1}{T} \sum_{t=1}^T (\Xi_k(t) - \mu_k)^2}}. \quad (1)$$

For our data, we only analyze $\Delta t = 10 \text{ min}$. A visual inspection of Fig. 2(a) shows an example of this property for one WT in a time period of two weeks. Apparently, increments of similar size cluster in time indicate some degree of correlation. This generally indicates that

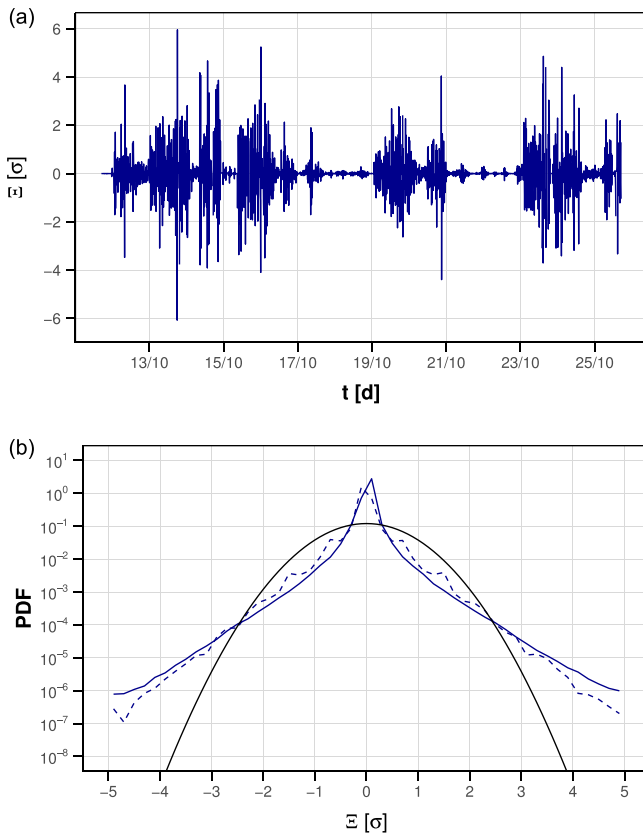


FIG. 2. Exemplary power increment time series covering two weeks and respective single-logarithmic histogram for all WTs covering the entire time period, compared to a Gaussian distribution. The dashed line includes power increments of the aggregated wind farm.

simple random walk models do not yield a sufficient description that captures the complex temporal correlations of time series. The power seems to fluctuate symmetrically but clearly in a non-Gaussian fashion as it can be seen in the PDF of all $\Xi_k(t)$ for the total time period in Fig. 2(b). Here, we compare the empirical distribution to a Gaussian (black) with the same mean value and standard deviation. For the aggregated wind farm, the strong fluctuations appear slightly dampened. These findings are in accordance with results in the literature for increments on even shorter timescales.⁸

If the PDF deviates from Gaussian statistics, we address the intermittent behavior after Kolmogorov 1962, expressed by a heavy tailed distribution and multifractal statistics. Note that this turbulent intermittency term is not the same as the alternative denotation of intermittency, i.e., nonstationary time series switching between different flow states such as between laminar and turbulent flows.

III. AUTOCORRELATION

Both the bimodality of power, persisting at values around zero and rated power output, and the complex dynamics of power increments suggest that an analysis of correlations can be fruitful. As the first step, we display linear autocorrelations for power time series $P_k(t)$.

To this extent, we use the Pearson correlation with a time delay τ defined by

$$\Theta(\tau) = [\langle X(t)X(t+\tau) \rangle_t - (\langle X(t) \rangle_t)^2] / \langle (X(t))^2 \rangle. \quad (2)$$

Quantifying autocorrelations of power time series yields valuable information on how power can be generally modeled (Sec. IV). In this paper, we only consider the autocorrelation of power time series. With $\Theta(\tau)$ as a correlation measure, we only account for linear dependence. Moreover, it is sensible to outliers and only gives sufficient information for time series with finite variance. Figure 3(a) shows $\Theta(\tau)$ for the power time series of all 30 WTs. It is shown up to a lag of seven days, which is approximately the point where they drop below a significant level (dashed horizontal lines). As such, we use a simple surrogate approach and shuffle the time series, eliminating temporal information but preserving the PDF. We identify a (constant) confidence band by calculating its width as 2σ of the autocorrelation after the shuffling process, averaged over all time series. The autocorrelation of all $P_k(t)$ slowly decreases over three orders of magnitude and thus indicates the long-range dependence. Nevertheless, $\Theta(\tau)$ does not show a typical power law decay but runs through several local maxima, reflecting the inherent nonstationarity. In Ref. 48, an explanation for this observation is provided, which corroborates our results: the autocorrelation of wind speed decreases with slightly visible maxima due to weather related seasonalities. Since power is closely coupled to wind speed and persists at an almost constant level for values around u_- and u_+ , the local maxima are not only sustained but amplified. The displayed autocorrelations do finally not show significant differences between single WTs even though it is known that relative positions of WTs play a role for power generation, e.g., through wind shear effects.⁴⁹ Such differences could potentially become visible in lagged cross-correlations between WTs of varying relative positions, which is not within the scope of this work though.

The scaling behavior of power time series is expected to be related to that of wind time series. For the latter, it is well known that the Fourier power spectrum obtained yields a power law decay $E(f) \propto f^{-\beta}$ with $\beta = 5/3$ estimated through linear regression in the log-log plot. This finding is in accordance with results one obtains from Kolmogorov's turbulence model. A simple way to confirm that a similar scaling can be found for the power time series, we estimate β from a respective Fourier power spectrum in Fig. 3(b). To this extent, we compute a smoothed spectrum (black) by splitting the full time series $P(t)$ of an exemplary WT into ten chunks and average over spectral power values obtained for each of the single segments (example in gray). The linear maximum likelihood estimation (MLE) regression (orange) yields $\beta = 1.58 \approx 5/3$ within a linear region of sufficient width and thus matches both the expected universal scaling (red) and results from similar data well.⁵⁰

The presence of nonstationarity leads to biased or spurious detection of autocorrelations.⁵¹ To uncover autocorrelations in the presence of nonstationary, we apply DFA⁵² to the power time series $P_k(t)$. The main idea of DFA is to eliminate nonstationarity in a generalized fashion by subtracting polynomial trends and consequently focusing on correlations that are present in the remaining noise. The method aims at calculating the Hurst exponent H , introduced by Hurst in 1951.⁵³ We distinguish between persistent ($0.5 < H < 1$) and antipersistent ($0 < H < 0.5$) behaviors of a time series. The special case $H = 0.5$

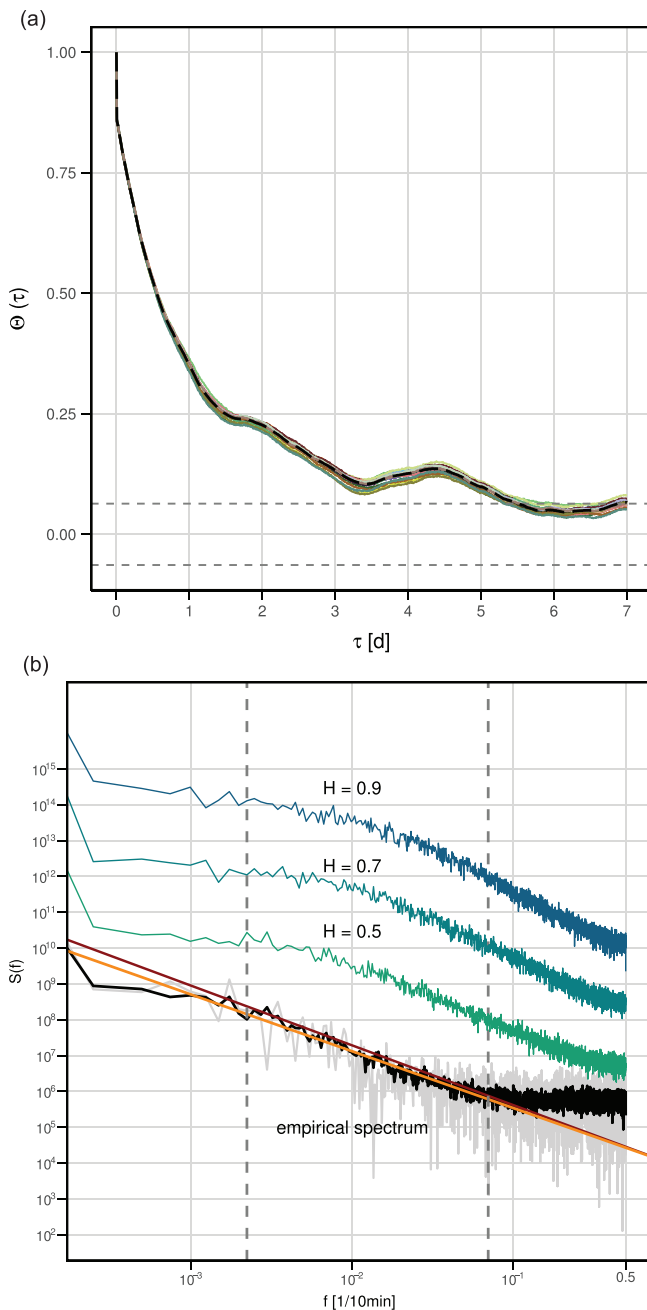


FIG. 3. Autocorrelation and Fourier spectrum of power time series. (a) $\Theta(\tau)$ for power time series of all 30 WTs for $\tau \leq 1$ week. The average autocorrelation is drawn as a black dashed line. The dashed horizontal lines represent a level of significance. (b) Fourier power spectrum of an exemplary power time series with a log-log-scale. The time series was split into ten equally sized segments for which the power spectra were computed (example: gray) and averaged subsequently (black). The orange line shows the linear regression performed within the fitted region (dashed lines), and the red line displays a scaling with $\beta = 5/3$. The three additional spectra are equivalently computed for the optimized model time series (see Fig. 8) with the respective Hurst exponent and shifted for better visibility.

yields diffusive behavior, i.e., uncorrelated white noise with $\langle X^H(t)X^H(t') \rangle = 0$ for the time series $X(t)$ at arbitrary times t and t' . Cumulated white noise entails Brownian motion. The persistent regime $H > 0.5$ results in super-diffusive dynamics and long-range dependence of the increments $X(t)$. Antipersistence yields the opposite case, i.e., a time series changes its direction more frequently than a diffusive time series. The respective extension of a white noise process is called fractional Gaussian noise (FGN) and will be addressed later.

We now briefly sketch the method of DFA and refer to Ref. 52 for a more detailed description. As a first step, we calculate the integrated, mean adjusted power time series. A time series of equal length is obtained, which is split into $N_s = \lfloor T/s \rfloor$ disjunct subsets of equal length s . The brackets round the value of T/s down to an integer value. We repeat this step with the reversed time series to incorporate all subsets. Subsequently, a polynomial quadratic detrending via MLE-regression (maximum likelihood estimation) is applied for all subsets. We then calculate the standard deviation $F_\nu(s)$ of all detrended subsets and from that derive the average standard deviation. Repeating this calculation for different s values, we obtain the fluctuation function

$$F(s) = \sqrt{\frac{1}{2N_s} \sum_{\nu=1}^{2N_s} F_\nu^2(s)}, \quad (3)$$

which represents the scale dependent fluctuation strength. We estimate the scaling exponent α from $F(s) \propto s^\alpha$ empirically via linear regression in a double-logarithmic plot since we expect $F(s)$ to increase as a power law. For stationary time series (e.g., FGN²²), we can identify α with the Hurst exponent H . In the more general case frequently encountered for real data, even for the detrended time series, some nonstationarity remains present. In this case, the Hurst exponent can only be estimated as $H \approx \alpha - 1$, which only strictly holds for a fractional Brownian motion (FBM) process. This distinction is sometimes not pointed out distinctively in the literature.⁵⁴ In general, α is also linked to the Fourier scaling exponent β via $\beta = 2\alpha - 1 = 1 + 2H$, enabling us to assess the consistency of our results.

For applications, s must not be chosen too small for a significant outcome. The DFA method is known to cause misleading finite size effects with respect to short timescales s , and the applied detrending generally needs to be regarded critically.⁵⁵ Another typical issue is values at the limits or outside of the range $0 < \alpha < 1$. For $\alpha > 1$, we have to consider the time series as an integrated process with more complex nonstationarities ($H = 1.5$ equals Brownian motion).^{56,57} Apart from this, the resulting increase in $F(s)$ does not have to be completely linear but can contain crossovers with different slopes.⁵⁸ In many cases, these crossovers are meaningful and uncover different scaling regions that entail different correlations.¹⁴ As we see in Fig. 4, the displayed fluctuation functions follow power laws with similar scaling exponents α . We checked that the displayed results are robust to different orders of polynomial detrending. Three shifted curves are shown for single WTs and one for the aggregated wind farm. A linear increase with one clearly visible crossover s_c at a timescale of approximately three days can be identified for all of the curves. The resulting scaling exponents are $\alpha = 1.33$ for $s \leq s_c$ and $\alpha = 0.80$ for $s > s_c$, averaged over all obtained α for different turbines. The values are almost identical for the aggregated wind farm. The dashed line emphasizes that all found results in fact give meaningful information about the correlations and the distribution. The line refers to a stationary random surrogate time

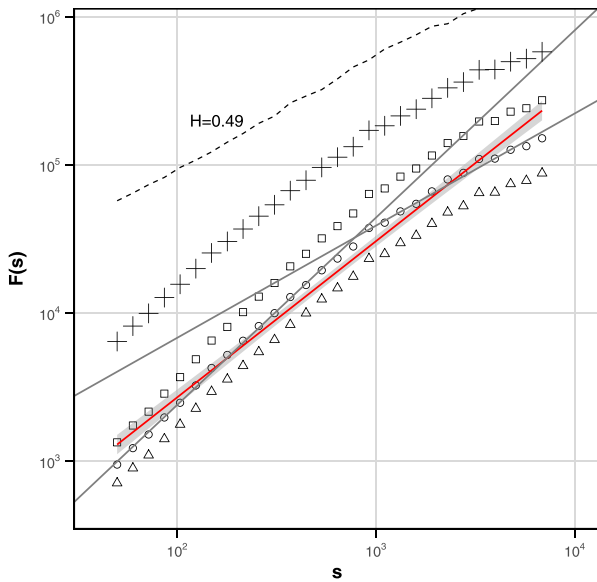


FIG. 4. Fluctuation function $F(s)$ for three exemplary WTs and aggregated WF (crosses). s is given in units of 10 min. The curves are shifted in the y -direction for better visibility. The red line displays the MLE-regression with the shaded error region. The gray lines visualize the crossover. The dashed line shows $F(s)$ for a surrogate of randomly shuffled data.

series we obtained with the same procedure explained above and applying DFA afterwards. A value of $H_{\text{surr}} = 0.49$ reflects diffusive behavior. Consequently, for short timescales $s \leq s_c$, the power time series have to be regarded as a highly nonstationary stochastic process with trends that cannot be sufficiently eliminated by DFA. If we suppose the validity of $H \approx \alpha - 1$ for $s \leq s_c$, we obtain $H \approx 0.33$ matching $H \approx 0.5(\beta - 1) = 0.29$ derived from the Fourier spectrum in Fig. 3(b). For $s > s_c$, the scaling exponent $\alpha = 0.80$ yields persistence and a Hurst exponent $H \approx -0.20$. The latter finding is consistent with the displayed autocorrelation functions and values of α found in the literature.^{24,29,50}

The same type of crossover behavior is also found for hourly wind speed data at geographically different sites.⁵⁴ The authors conjecture that this scaling behavior might arise from the different scales of weather patterns, which would manifest itself in a multifractal spectrum of different scaling exponents. Yet, the crossover is not critically reflected on, even though misleading crossovers in DFA are known to appear with several known causes. In Ref. 14, it is suggested to test whether different orders of polynomial detrending change the crossover position, which we ensured not to occur. Furthermore, the number of NA-values does not have a significant impact on our results as supposed in Ref. 59. Although the scaling law of $F(s)$ is still valid for $\alpha > 1$,⁵⁷ this special case hints that unidentified trends remain after the detrending procedure. Such trends are also known as a source of erroneous crossovers,^{60,61} which we cannot fully rule out. If such trends were the cause, similar trends would also be present in the wind speed data in Ref. 54 though. The consequences of such a crossover still seem to be of potential importance for possible modeling approaches, which will be addressed in Sec. IV.

IV. STOCHASTIC MODEL

The identified features of single WT power time series motivate a model approach that could be calibrated with empirical data. We now put forward such a time series modeling approach that has the potential to be used in a larger simulation, aiming at a multi-scale model of wind power generation. In Sec. IV A, we introduce our model approach. We compare our model results to the empirical data in Sec. IV B to gain first qualitative insights into the scope of the model.

A. Model approach

Numerous approaches of power time series $P(t)$ simulations are employed in the literature. A major fraction tends to simulate wind farm power time series only and does not concentrate on single WTs as we intend to do.^{35,62–64} Another central distinction is the aim of the model. Our reduced-form approach does not intend to reproduce temporally ordered forecasts but only statistical features such as distributions and long-term averages. Several models in the literature manage to give precise forecasts of different time horizons of $P(t)$ using black-box models with a high number of parameters or simple regression parameters that often lack a comprehensive contextual meaning. Typical model approaches in this context are Markov processes^{48,65,66} and ARIMA (autoregressive integrated moving average) processes,³⁷ both of which focus on the autocorrelation of $P(t)$. Further approaches are based on nonlinear models,⁶⁷ stochastic models,⁴³ and stochastic drift-diffusion-models.²⁰ In contrast to the stochastic process approach in Ref. 20, which aims to model the stochastic wind speed/wind power relation in seconds by the estimators of Kramers–Moyal coefficients, we aim here to achieve a stochastic modeling of the power output based on 10 min values.

We will try to introduce our model parameters with a comprehensible meaning. Furthermore, our model equation itself is not a regression formula but is based on our qualitative understanding of power time series. The simulations are carried out on a 10-min timescale. The essence of our model comes down to one fundamental stochastic differential equation (SDE) based on central statistical features we identified in Secs. II and III. We do not model NA-values separately and aim at simulating the raw uncleaned data that are directly obtained from the SCADA system.⁶⁸ For the sake of simplicity, all model-related equations are formulated in a notation for continuous systems, yet bearing in mind that we are dealing with discrete data. We now briefly introduce the stochastic model equation and summarize the related mathematical concepts. In our modeling framework, we will regard power generation as an autocorrelated stochastic process with a deterministic and a stochastic component. These drift-diffusion-types of models are often expressed by a Langevin equation of the general form

$$\frac{dP}{dt}(t) = -k \frac{dV(P)}{dP} + D \xi_H(t). \quad (4)$$

Here, $P(t)$ denotes the power time series. The first term equals the deterministic drift component with a drift parameter k and a potential function $V(P)$. The second component incorporates stochastic fluctuations $\xi_H(t)$ with a constant diffusion strength D . The index H denotes the Hurst exponent, which hints at the fact that we can include arbitrary power law-like correlations into our model. Thus,

$\xi_H(t)$ itself is a solution to a simple FGN-stochastic process⁶⁹ with the defining property

$$\langle \xi_H(t) \xi_H(t') \rangle = \frac{1}{2} (|t|^{2H} + |t'|^{2H} - |t - t'|^{2H}). \quad (5)$$

In this way, we can transfer our empirical knowledge about the autocorrelation of $P(t)$ from Sec. III to the model approach. Furthermore, we choose the deterministic potential function $V(P)$ in a way that focuses on the time series dynamics around the fundamental fixed points. Since we have observed that power generation mostly concentrates around zero power output P_- and rated power P_+ , we choose a bimodal approach with the double-well potential function

$$V(P) = \frac{1}{4a^4} (P - P_0)^4 - \frac{1}{2a^2} (P - P_0)^2. \quad (6)$$

While a describes the steepness of the potential, P_0 gives us the position at which it is centered. Such SDEs are used in different applications in the literature and are referred to as a description of an overdamped Brownian particle in a double-well potential⁷⁰ in statistical physics. As an illustration, we can think of the underlying dynamics as a particle that would jump between the potential minima, driven by correlated fluctuations. The latter consequently introduce a characteristic timescale for the transitions between the fixed points. Often, such models are extended by a driving periodical force that entails a biased occupation of one fixed point with respect to a certain seasonality. Since power generation from wind energy follows seasonal variations, we incorporate this into our model with the simple approach

$$F(t) = A \cos \omega t, \quad (7)$$

which is added to Eq. (4) as the driving force. We determine ω from Fourier analysis as the leading frequency within the spectrum of $P(t)$. A gives us the adaptable strength of the seasonal variations. With this extension, we introduce another characteristic timescale into our approach. The interplay of both this component and the stochastic fluctuations determines the transition dynamics as described by the general phenomenon of stochastic resonance.⁷¹ Our approach effectively biases the bimodal PDF of modeled power toward one of its peaks, which reproduces the seasonal variation of wind power generation on a rather basic level. In the parameter estimation of ω , we incorporate data from a specific month to calibrate the seasonality according to the month in the data.

As we have seen in Fig. 1, the control of the WTs results in extremely narrow peaks of the PDF of $P(t)$. This fact is caused by the intervening external control of power output (curtailment). Our model approach already succeeds to concentrate the power values around P_- and P_+ as fixed points in a similar manner but fails to narrow the peaks down as sharply as required due to the simple analytical approach. Hence, we have to incorporate the artificial flattening of time series we observe in the data into our model sufficiently. To do so, we cut off power values beyond the operating range $P_- \leq P \leq P_+$ by setting them to the respective constant threshold value P_- or P_+ . As we observe in the data, these limits are sometimes exceeded in the empirical time series anyway. Consequently, this procedure is only applied with a certain probability p_{\geq} . Note that the model cannot be regarded as a typical Langevin-equation driven model since the correlated noise term $\xi_H(t)$ on the one hand and the artificial flattening due to curtailment on the other hand differ strongly from the standard

delta-correlation of such models. Taking all explained considerations of our model approach into account, the resulting model formula is

$$P(t) = \begin{cases} \tilde{P}(t) & \text{if } P_- \leq P(t) \leq P_+ \\ P_{\pm} & \text{if } \tilde{P}(t) \geq P_{\pm} \text{ with } p = 1 - p_{\geq} \\ P_{\pm} + z & \text{if } \tilde{P}(t) \geq P_{\pm} \text{ with } p_{\geq}, \end{cases}$$

$$\frac{d\tilde{P}(t)}{dt} = \left[- \left(\frac{\tilde{P}(t) - P_0}{a} \right)^3 + \frac{\tilde{P}(t) - P_0}{a} + A \cos \omega t \right] + D \xi_H(t), \quad (8)$$

with the respective probabilities p_{\geq} for having a power value beyond the operation range and a $\mathcal{N}(0, \sigma)$ -distributed random number z . The model includes ten parameters in total. A detailed description of the parameter calibration and all resulting values are given in Appendix. Six parameters (P_0 , ω , p_{\geq} , σ_{\geq}) are calibrated on the data before a time series is to be modeled. P_0 determines around which power value the distribution of values should be centered. The frequency ω should include some limited degree of season-specific variations and is fixed via Fourier analysis. The remaining four parameters p_{\geq} and σ_{\geq} calibrate the curtailment and variability of power beyond the operating range. The three parameters a , A , and D are optimized such that the model reproduces the empirical statistical features most effectively while avoiding overfitting. The Hurst exponent H will be varied in Sec. IV B to observe how different autocorrelations affect the generated power.

B. Results

We get a first glance of the model results by inspecting simulated time series. We vary the Hurst exponent H from diffusive ($H=0.5$) to persistent ($H=0.7$) up to strongly persistent ($H=0.9$) dynamics to account for different degrees of correlation within the model. Thus, our approach does not incorporate the uncovered crossover behavior that would separate between different autocorrelations below and above s_c but only account for scales $s < s_c$ in the stochastic component. Yet, the deterministic component results in strong ramps that are intended to resemble the observed power ramps that lead to the Hurst exponent $H > 1$ for $s > s_c$. We always compare the simulated results to only one exemplary WT since the model aims at characterizing the typical dynamics instead of a single specific WT. Figure 5 shows three randomly chosen numerical time series $P(t)$ with different Hurst exponents and compares them to one empirical time series at the bottom. A visual inspection gives a first indication of the similarity between the empirical results from Sec. III and the modeled time series. For $H=0.9$, the modeled time series reproduces both the transitions between P_- and P_+ and the fluctuations around local trends most accurately. The strong abrupt ramps on short timescales can also be observed for all modeled time series. Note that if power time series had uncorrelated fluctuations (red curve), they would apparently tend to change their local trend more frequently.

After this first visual comparison, we next present a more quantitative comparison of the model and empirical data. Therefore, we consider the bimodality of power statistics, the intermittent behavior of the increment statistics, and both the autocorrelation and power spectra of power time series.

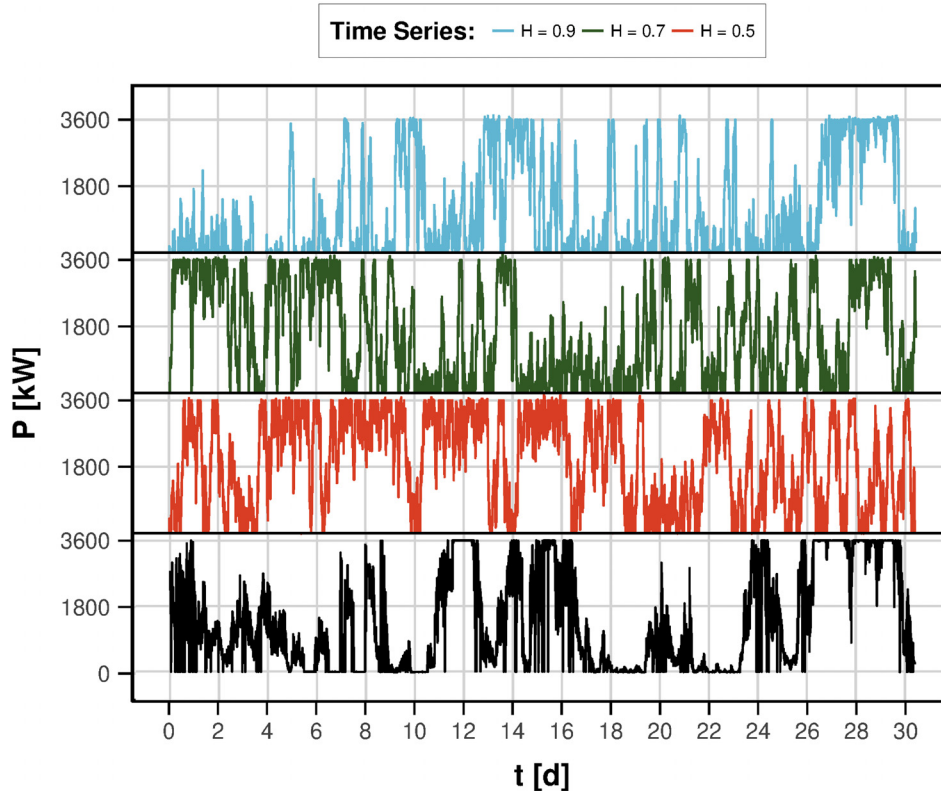


FIG. 5. Comparison between empirical (bottom) and simulated power time series for different Hurst exponents H . The black line represents a typical empirical time series for one month. The simulated time series are generated for the same month and chosen randomly.

The quality of the reproduced PDF shown in Fig. 6 for different values of H is not as obvious. This time we choose the sampled time series $P(t)$ whose PDF reproduces the height of the bimodal peaks most sufficiently but still reflects a typical result. While the PDF for $H = 0.9$ reproduces the bimodality of the power time series in a satisfactory manner, the average values (dashed line) clearly differ. For $H = 0.5$, peak heights cannot be reproduced: a sample of $P(t)$ with uncorrelated fluctuations tends to occupy both fixed points P_- and P_+ with the same frequency. This behavior is entailed by the enhanced frequency of transitions we observed in Fig. 5. Yet, it fails to give a convincing result for the mean value even though it should be more stably centered for a balanced PDF.

The power increments $\Xi_k(t)$ are an essential quantity for the control of WTs and grid stability. Besides the analysis in terms of autocorrelation and power spectra of $P_k(t)$ (see below), higher statistical features of the power fluctuations can be grasped by investigating the statistics of the power increments, yielding higher order statistical features of power fluctuations. A comparison of increment statistics between real and modeled data can display strengths and weaknesses of the model to capture the intermittent nature of power generation, expressed by strong correlated fluctuations. To this extent, we compare the quantiles of the model results for the power increments with the empirical data. This empirical test clarifies qualitatively in which way the two distributions generally differ regarding their quantiles.

Since our model captures the effect of different degrees of autocorrelation for the power time series with the Hurst parameter H , we can also study the effect of autocorrelation in the power time series on

the increment statistics and possible non-Gaussian characteristics. In Fig. 7, the quantiles of three simulated power time series with varied H are plotted against the quantiles of an empirical power time series. If they were equally distributed, they would follow the diagonal black line. It becomes apparent that in the strongly persistent regime of $H = 0.9$, the larger increments that possess the non-Gaussian property are reproduced most sufficiently. Increments up to $|\Xi_k(t)| < 4\sigma$ are almost equally distributed to the randomly chosen empirical time series. The deviations mostly occur in the heavy tails of the distributions for larger absolute increments. Small increments $|\Xi_k(t)| < \sigma$ are not adequately described by any of the sampled time series. We point out that the shape of the QQ-curve for persistent samples $P(t)$ with $H = 0.7$ differs only slightly from the one with $H = 0.5$.

From this, we conclude that a certain threshold of persistence has to be exceeded so that big jumps between P_- and P_+ dominate and generate strong heavy tails. Thus, the persistence of power is closely related to its intermittent behavior regarding its fluctuations. The results we compared so far demonstrated that the model successfully reproduces important statistical characteristics of power generation with respect to the statistical distribution. The variation of Hurst exponents as a tool to incorporate the temporal correlation of power time series should yet yield a strong impact on the autocorrelation function. Thus, we analyze how well the autocorrelation function $\Theta(\tau)$ and also the power spectrum are reproduced by our model. Figure 8 shows in black the monthly averaged autocorrelation of empirical power time series. We compare autocorrelations for the three different Hurst exponents in the same average. The model in general succeeds to

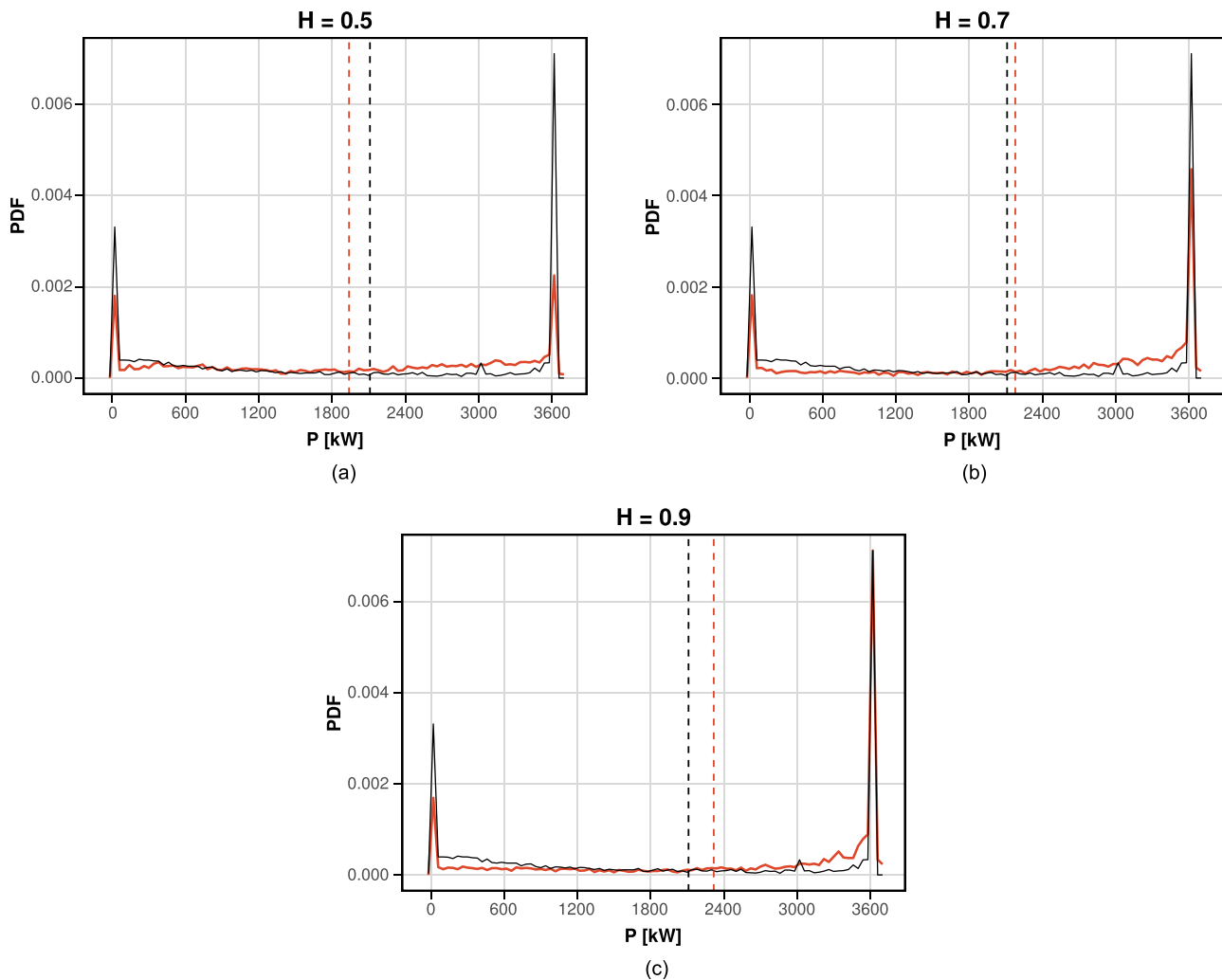


FIG. 6. Comparison between the PDF of empirical (black) and simulated (orange) power time series for one exemplary month. The Hurst exponent H is varied for every histogram. The dashed lines indicate the respective average power values.

reproduce the slowly decreasing autocorrelation with a decay on the same timescale. Although we observe the expected relation that higher values of H lead to a more slowly decaying autocorrelation, none of the model results yields a sufficient reproduction of the decay for $\tau \leq 1$ d. Only for $H = 0.9$, the simulated autocorrelation approaches the empirical one within this interval. In general, the results for $\tau > 1$ d are more applicable and even tend to reproduce the weak anticorrelation for $\tau > 5$ d. The discussed seasonal bumps are not clearly distinguishable for any of the model results. The model autocorrelations show stronger fluctuations, which indicates that the monthly average does not cancel out the impact of monthly varying timescales as much as for the empirical data. A more sophisticated approach for the seasonal component in our model could enhance this aspect.

Finally, Fig. 3(b) shows the three corresponding averaged power spectra for the model time series (green). In contrast to the empirical

spectrum, the slope remains almost constant for all H values even beyond the cut-off value (dashed line), yielding lower power for higher frequencies. Within the fitted region, all three spectra show a qualitatively similar decay with $\beta \approx 5/3$. In particular, the time series with the highest persistence again gives the most convincing result ($H = 0.5: \beta = 1.71 \pm 0.03$, $H = 0.7: \beta = 1.69 \pm 0.04$, $H = 0.9: \beta = 1.64 \pm 0.03$).

V. CONCLUSION

We analyzed a dataset comprising a time series of 30 WT's located at the German offshore wind farm RIFFGAT over a total time period of one year. As important basic features, we found power values of each WT to be bimodally distributed with density peaks at zero power output P_- and rated power output P_+ . The power output $P_k(T)$ of a WT turned out to have a slowly decreasing autocorrelation, which connects to general findings in the literature. Beyond these basic

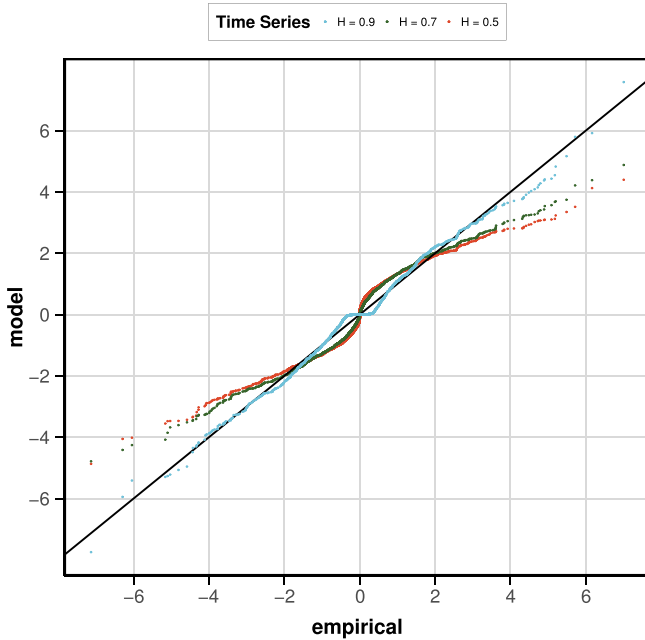


FIG. 7. Direct comparison between empirical and simulated distributions of power increments $\Delta(t)$ in a QQ-plot for different Hurst exponents H . The ordinate shows the quantiles of the modeled distribution, and the abscissa shows those of the empirical distribution. The black diagonal line serves as a reference for an equal distribution of both.

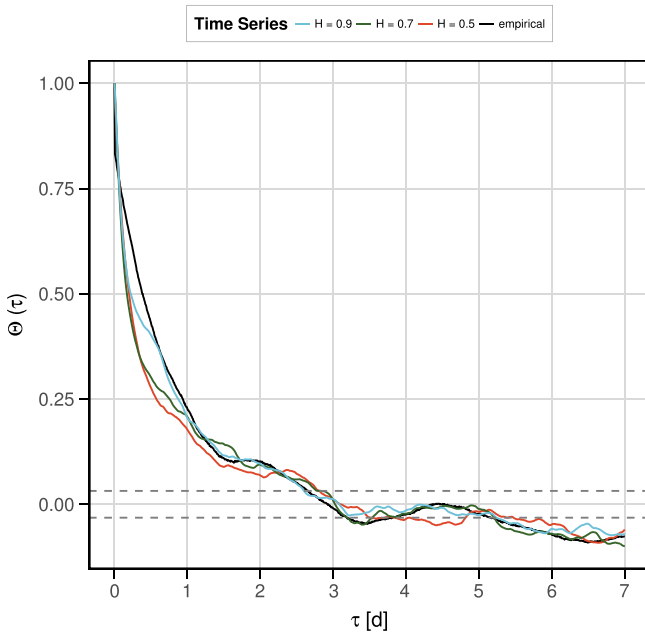


FIG. 8. Comparison between the autocorrelation $\Theta(\tau)$ of empirical and simulated power time series for different Hurst exponents H . The maximum delay τ is one week. The dashed horizontal lines represent the averaged level of significance.

features, we took into account the non-stationarity of time series by applying DFA to both $P_k(T)$. In terms of the Hurst exponent as a general classifier for autocorrelations of single WTs, different characteristic timescales were identified on which correlations vary between persistence and more involved nonstationarity, separated by a crossover $s_c \approx 3$ d. Based on these findings, we put forward a reduced form model for the power output $P_k(t)$. With this model, we intended to provide a tool for reproducing several statistical properties and testing power generation scenarios with respect to empirically motivated parameters. To this extent, we employed a nonlinear stochastic differential equation with a double-well potential and a correlated diffusion component. Most parameters were estimated empirically, while some were optimized to capture statistical properties of the data. The model succeeded to qualitatively reproduce important statistical characteristics such as a bimodal PDF, intermittent fluctuations, and a slowly decreasing autocorrelation. It thus enriches the modeling perspective on power generation by focusing on a comprehensive set of statistical features only while still producing characteristic results. Possible applications include wind farm or large power network simulations that still aim at reflecting single WT dynamics adequately. Even for such aggregated large-scale approaches, taking correlations on a single WT scale into account is essential since models with uncorrelated fluctuations will underestimate important statistical effects such as heavy tailed distributions and persistence.

Anyway, the proposed model should be regarded as the first step toward a study that quantitatively reflects on the model dynamics in greater detail and undermines the significance of the obtained results. While a systematic examination of parameter effects on the outcome remains to be done, some parameter estimation methods could also be subject to further improvement. The observed crossover that uncovers different correlations on timescales $t \leq 3$ d could be of interest for possible model extensions. The strong ramping behavior on short timescales, which is suspected to entail the found crossover, is an important component in the context of predictability despite strong intermittent fluctuations. Finally, we only focused on single WTs. An evident extension of the proposed model would be to aggregate several correlated single WTs⁷² and wind farms⁷³ model power outputs and study characteristics of aggregated output,⁷² especially with regard to an amplification of correlated fluctuations at the aggregated level.

ACKNOWLEDGMENTS

Part of this work was financially supported by the Ministry for Science and Culture of the Federal State of Lower Saxony within the project “Ventus Efficiens” under Grant No. ZN3024. We further acknowledge support from the Open Access Publication Fund of the University of Duisburg-Essen.

APPENDIX: PARAMETER ESTIMATION

We briefly provide an overview of the model parameters and explain the methods of how they are calibrated. To solve the SDE, we use the Euler–Maruyama-method for SDEs with colored noise.⁷⁴ We sample the latter by using the so-called Harte-method, applying the Durbin–Levinson-algorithm.⁷⁵ Averaged over 10 000 samples, it

takes us 0.095 ± 0.009 s to simulate a power time series covering a period of one month with the hardware setup used in this study. One advantage of our model lies in the fact that we can already fix six of ten parameters before we simulate a single time series only by adjusting them in a particular way to the empirical data. Consequently, the estimation of these six fitted parameters is enhanced, and more data are included. This data based approach enables us to assign interpretations to the parameters in context of the empirical data

- Center of potential function P_0 : the most apparent value for the center of the symmetric double-well potential P_0 is to fix it at the center of the empirical range of power values $P_0 = 1800$ kW. This choice simply ensures that for an appropriate choice of a , the model reproduces the bimodal peaks at the correct power output.
- Seasonal frequency ω : since we introduced the frequency ω of the periodical driving force into our model to include seasonal variations, we estimate it from the empirical wind speed time series $u(t)$ by applying Fourier analysis. By choosing ω to be the Fourier frequency of the highest Fourier amplitude, we make sure that it at least resembles the most dominant seasonal frequency in the data. We choose the wind speed time series $u(t)$ instead of the power times $P(t)$ because we regard $u(t)$ to be the external drive for the WTs analogously to an external driving force of a periodically driven oscillator. This simple approach can only account for a rough estimation of the seasonal variations.
- Probabilities for excess/negative power p_{\geq} : both parameters need to be set with respect to the likelihood of empirical power values beyond the operating range. A power lower than P_- or higher than P_+ can only be generated if the corresponding wind speed u is lower than u_- or higher than u_+ , respectively. Hence, we calculate the probabilities for such wind speed values from the empirical data and use these probabilities to fix the model probabilities p_{\geq} . Since these probabilities show significant variations between different months, we obtain 24 values in total that can be interpreted as the monthly likelihood for the WT to generate power beyond its operating range.
- Standard deviation for excess/negative power σ_{\geq} : how strongly does power fluctuate around P_- and P_+ when this range is exceeded?—As we already stated, we choose a simple Gaussian distribution for the power values around these two values. We fix σ_{\geq} applying a Gaussian empirical fit around P_- and P_+ , respectively. Since this empirical standard deviation hardly varies for different months, we only obtain the two values $\sigma_+ = 68.93$ kW and $\sigma_- = 4.47$ kW.

The remaining four parameters should be regarded as more dynamical parameters that we try to estimate by optimizing a certain statistical feature with respect to this parameter. One exception is the Hurst exponent H that we vary between the three values $H = 0.5, 0.7, 0.9$ in Sec. IV B toward a better understanding of the impact of power law autocorrelations on power generation. We briefly sketch the estimation methods for the parameter a of the potential function, the diffusion strength D , and the strength of the seasonal variation A . For each parameter, we optimize it by sampling a reasonable number of time series for each of the 12 months.

- Curtailment indicator a : after we have set $P_0 = 1800$ kW, the most obvious choice for a would also be $a = 1800$ kW to ensure that the bimodal peaks center around the correct fixed points $P_- = 0$ kW and $P_+ = 3600$ kW. Anyway, the artificial flattening procedure plays an important role in this context: if we choose $a = 1800$ kW, the amount of values that are either set to one of the thresholds P_- or P_+ or scattered around them is too high compared to the empirical data. This hints at choosing a value $a < 1800$ kW. We optimize a by sampling power time series with different $a < 1800$ kW and calculating the amount p_{\geq} of power values above (below) or around P_+ (P_-). The resulting value (for fixed H) minimizes the difference between the respective empirical and simulated values. Consequently, we regard the difference $(P_0 - a)$ as the power difference that entails how strongly the empirical power time series are subject to curtailment.
- Diffusion strength D : the constant diffusion strength D determines how strongly the stochastic component dominates power generation. It is an important parameter in the context of transition timescales between the two fixed points P_- and P_+ . If we regard $D\zeta_H(t)$ as the diffusion function of a Langevin equation, we can apply the standard method to obtain this diffusion function directly from the empirical data.⁷⁶ It can be shown⁷⁷ that the diffusion function can be extracted by calculating

$$D^{(2)}(P, t) = \lim_{\tau \rightarrow 0} \frac{\langle (P(t + \tau) - P(t))^2 \rangle}{\tau} \Big|_{P(t)=P_0} \quad (A1)$$

Since this method potentially yields erroneous results for correlated noise processes, we can only expect an approximate estimate of D .⁷⁸ Nevertheless, we follow this approach by minimizing the difference $\min_D [|D_2^{\text{emp}}(P(t)) - D_2^{\text{sim}}(P(t); D)|]$ of the empirical and the model diffusion function with respect to D .

- Seasonal variation strength A : A biases the power generation toward one of the two peaks of the bimodal power distribution. In winter months, a high average power output is likely, whereas in spring, usually lower wind speeds occur, which lead to a pronounced peak around P_- . Thus, we can calculate

$$E(t) = \sum_{t'=t_0}^t P(t'), \quad (A2)$$

resembling an energy indicator for the empirical and simulated data to minimize the difference between the respective time-averaged values $\langle E(t) \rangle_t$. We consider A to be optimized when this difference of averaged accumulated power values is minimized for each month.

We summarize the parameter choices we obtain from the above-mentioned estimation methods (Table I).

TABLE I. Estimated parameters for different Hurst exponents H .

H	a (kW)	D (kW/ \sqrt{s})	A (kW/s)
0.5	1755	355	0.15
0.7	1445	360	0.17
0.9	1235	485	0.26

REFERENCES

- ¹F. Appavou, A. Brown, B. Epp, D. Gibb, B. Kondev, A. McCrone, H. E. Murdock, E. Musolino, L. Ranalder, J. L. Sawin, K. Seyboth, J. Skeen, and F. Sverrisson, *Renewables 2019 Global Status Report* (REN21 Secretariat, Paris, 2019).
- ²X. Lu, M. McElroy, and J. Kiviluoma, "Global potential for wind-generated electricity," *Proc. Natl. Acad. Sci.* **106**, 10933–10938 (2009).
- ³P. Crossley and A. Beviz, "Smart energy systems: Transitioning renewables onto the grid," *Renewable Energy Focus* **11**, 54–59 (2010).
- ⁴J. M. Carrasco, L. G. Franquelo, J. T. Bialasiewicz, E. Galván, R. C. Portillo Guisado, M. Á. Martín Prats, J. I. León, and N. Moreno-Alfonso, "Power-electronic systems for the grid integration of renewable energy sources: A survey," *IEEE Trans. Ind. Electron.* **53**(4), 1002–1016 (2006).
- ⁵Z. Jiang, Q.-S. Jia, and X. Guan, "Review of wind power forecasting methods: From multi-spatial and temporal perspective," in *2017 36th Chinese Control Conference (CCC)* (IEEE, 2017), pp. 10576–10583.
- ⁶S. S. Soman, H. Zareipour, O. Malik, and P. Mandal, "A review of wind power and wind speed forecasting methods with different time horizons," in *North American Power Symposium 2010* (IEEE, 2010), pp. 1–8.
- ⁷G. Ren, J. Wan, J. Liu, D. Yu, and L. Söder, "Analysis of wind power intermittency based on historical wind power data," *Energy* **150**, 482–492 (2018).
- ⁸M. Anvari, G. Lohmann, M. Wächter, P. Milan, E. Lorenz, D. Heinemann, M. R. R. Tabar, and J. Peinke, "Short term fluctuations of wind and solar power systems," *New J. Phys.* **18**, 063027 (2016).
- ⁹C. M. S. Martin, J. K. Lundquist, and M. A. Handschy, "Variability of interconnected wind plants: Correlation length and its dependence on variability time scale," *Environ. Res. Lett.* **10**, 044004 (2015).
- ¹⁰W. Katzenstein, E. Fertig, and J. Apt, "The variability of interconnected wind plants," *Energy Policy* **38**, 4400–4410 (2010).
- ¹¹J. Heitzig, N. Fujiwara, K. Aihara, and J. Kurths, "Interdisciplinary challenges in the study of power grid resilience and stability and their relation to extreme weather events," *Eur. Phys. J. Spec. Top.* **223**, 2383–2386 (2014).
- ¹²L. R. Gorbão, M. Anvari, H. Kantz, C. Beck, D. Witthaut, M. Timme, and B. Schäfer, "Data-driven model of the power-grid frequency dynamics," [arXiv:1909.08346](https://arxiv.org/abs/1909.08346) (2019).
- ¹³Y. Stepanov, P. Rinn, T. Guhr, J. Peinke, and R. Schäfer, "Stability and hierarchy of quasi-stationary states: Financial markets as an example," *J. Stat. Mech.: Theory Exp.* **2015**, P08011.
- ¹⁴J. Kantelhardt, E. Koscielny-Bunde, H. H. Rego, S. Havlin, and A. Bunde, "Detecting long-range correlations with detrended fluctuation analysis," *Physica A* **295**, 441–454 (2001).
- ¹⁵A. N. Kolmogorov, "The local structure of turbulence in incompressible viscous fluid for very large Reynolds numbers," *C. R. Acad. Sci. URSS* **30**, 301–305 (1941).
- ¹⁶U. Frisch and A. N. Kolmogorov, *Turbulence: The Legacy of an Kolmogorov* (Cambridge University Press, 1995).
- ¹⁷R. Calif, "Pdf models and synthetic model for the wind speed fluctuations based on the resolution of Langevin equation," *Appl. Energy* **99**, 173–182 (2012).
- ¹⁸R. Calif and F. G. Schmitt, "Modeling of atmospheric wind speed sequence using a lognormal continuous stochastic equation," *J. Wind Eng. Ind. Aerodyn.* **109**, 1–8 (2012).
- ¹⁹R. Baïle, P. Poggi, and J.-F. Muzy, "Intermittency model for surface layer wind speed fluctuations: Applications to short term forecasting and calibration of the wind resource," in *Proceedings of EWEC* (2010).
- ²⁰P. Milan, M. Wächter, and J. Peinke, "Stochastic modeling and performance monitoring of wind farm power production," *J. Renewable Sustainable Energy* **6**, 033119 (2014).
- ²¹E. Fertig, J. Apt, P. Jaramillo, and W. Katzenstein, "The effect of long-distance interconnection on wind power variability," *Environ. Res. Lett.* **7**, 034017 (2012).
- ²²M. S. Taqqu, V. Teverovsky, and W. Willinger, "Estimators for long-range dependence: An empirical study," *Fractals* **3**, 785–798 (1995).
- ²³R. Kavasseri and R. Nagarajan, "A multifractal description of wind speed records," *Chaos, Solitons Fractals* **24**, 165–173 (2005).
- ²⁴R. Govindan and H. Kantz, "Long-term correlations and multifractality in surface wind speed," *Europhys. Lett.* **68**, 184 (2004).
- ²⁵L. Telesca and M. Lovallo, "Analysis of the time dynamics in wind records by means of multifractal detrended fluctuation analysis and the Fisher–Shannon information plane," *J. Stat. Mech.: Theory Exp.* **2011**, P07001.
- ²⁶P. Wei, J. Liu, Q. Zhou, and X. Zhu, "Multidimensional wind power correlation analysis and modeling based on pair copula," *DEStech Trans. Environ., Energy Earth Sci.* **10**, 3870–3882 (2018).
- ²⁷R. Calif and F. G. Schmitt, "Multiscaling and joint multiscaling description of the atmospheric wind speed and the aggregate power output from a wind farm," *Nonlinear Processes Geophys.* **21**, 379–392 (2014).
- ²⁸P. Milan, M. Wächter, and J. Peinke, "Turbulent character of wind energy," *Phys. Rev. Lett.* **110**, 138701 (2013).
- ²⁹L. McArthur, S. Mackenzie, and J. Boland, "Multifractal analysis of wind farm power output," in *Proceedings of the 20th International Congress on Modelling and Simulation, MODSIM, MSSANZ* (2013).
- ³⁰X. Wang, P. Guo, and X. Huang, "A review of wind power forecasting models," *Energy Procedia* **12**, 770–778 (2011).
- ³¹S. Kolumbán, S. Kapodistria, and N. Noorae, "Short and long-term wind turbine power output prediction," [arXiv:1707.06497](https://arxiv.org/abs/1707.06497) (2017).
- ³²J. Gottschall and J. Peinke, "How to improve the estimation of power curves for wind turbines," *Environ. Res. Lett.* **3**, 015005 (2008).
- ³³M. Cui, V. Krishnan, B.-M. Hodge, and J. Zhang, "A copula-based conditional probabilistic forecast model for wind power ramps," *IEEE Trans. Smart Grid* **10**(4), 3870–3882 (2018).
- ³⁴J. Jeon and J. W. Taylor, "Using conditional kernel density estimation for wind power density forecasting," *J. Am. Stat. Assoc.* **107**, 66–79 (2012).
- ³⁵P. Sørensen, A. Hansen, and P. Rosas, "Wind models for simulation of power fluctuations from wind farms," *J. Wind Eng. Ind. Aerodyn.* **90**, 1381–1402 (2002).
- ³⁶M. Yang, X. Chen, and B. Huang, "Ultra-short-term multi-step wind power prediction based on fractal scaling factor transformation," *J. Renewable Sustainable Energy* **10**, 053310 (2018).
- ³⁷P. Chen, T. Pedersen, B. Bak-Jensen, and Z. Chen, "ARIMA-based time series model of stochastic wind power generation," *IEEE Trans. Power Syst.* **25**, 667–676 (2010).
- ³⁸P. Hänggi and P. Jung, "Colored noise in dynamical systems," *Adv. Chem. Phys.* **89**, 239–326 (1995).
- ³⁹B. Lotfi, M. Mourad, M. Najiba, and E. Mohamed, "Treatment methodology of erroneous and missing data in wind farm dataset," in *2011 8th International Multi-Conference on Systems, Signals and Devices (SSD)* (IEEE, 2011), pp. 1–6.
- ⁴⁰Y.-H. Wan, "Wind power plant behaviors: Analyses of long-term wind power data," Technical Report No. US200430%909 (National Renewable Energy Laboratory, Golden, CO, USA, 2004).
- ⁴¹J. F. Manwell, J. G. McGowan, and A. L. Rogers, *Wind Energy Explained: Theory, Design and Application* (John Wiley & Sons, 2010).
- ⁴²H.-J. Wagner, "Introduction to wind energy systems," *EPJ Web Conf.* **54**, 01011 (2013).
- ⁴³T. Scholz, V. V. Lopes, P. Lind, and F. Raischel, "Modeling and analysis of cyclic inhomogeneous Markov processes: A wind turbine case study," [arXiv:1404.0203](https://arxiv.org/abs/1404.0203) (2014).
- ⁴⁴A. Muñoz, E. Sánchez-Úbeda, A. Cruz, and J. Marín, "Short-term forecasting in power systems: A guided tour," *Handbook of Power Systems II* (Springer, 2010), pp. 129–160.
- ⁴⁵W.-G. Früh, "From local wind energy resource to national wind power production," *AIMS Energy* **3**, 101–120 (2015).
- ⁴⁶N. Zhang, C. Kang, D. Kirschen, Q. Xia, W. Xi, J. Huang, and Q. Zhang, "Planning pumped storage capacity for wind power integration," *IEEE Trans. Sustainable Energy* **4**, 393–401 (2013).
- ⁴⁷F. Ziel, C. Croonenbroeck, and D. Ambach, "Forecasting wind power—modeling periodic and non-linear effects under conditional heteroscedasticity," *Appl. Energy* **177**, 285–297 (2016).
- ⁴⁸G. Papaefthymiou and B. Klockl, "MCMC for wind power simulation," *IEEE Trans. Energy Convers.* **23**, 234–240 (2008).
- ⁴⁹B. Wen, S. Wei, K. Wei, W. Yang, Z. Peng, and F. Chu, "Power fluctuation and power loss of wind turbines due to wind shear and tower shadow," *Front. Mech. Eng.* **12**, 321–332 (2017).
- ⁵⁰O. D. Medina, F. G. Schmitt, and R. Calif, "Multiscale analysis of wind velocity, power output and rotation of a windmill," *Energy Procedia* **76**, 193–199 (2015).

- ⁵¹J. Gao, J. Hu, W.-W. Tung, Y. Cao, N. Sarshar, and V. Roychowdhury, "Assessment of long-range correlation in time series: How to avoid pitfalls," *Phys. Rev. E* **73**, 016117 (2006).
- ⁵²A. Bashan, R. Bartsch, J. Kantelhardt, and S. Havlin, "Comparison of detrending methods for fluctuation analysis," *Physica A* **387**, 5080–5090 (2008).
- ⁵³H. Hurst, "The problem of long-term storage in reservoirs," *Hydrol. Sci. J.* **1**, 13–27 (1956).
- ⁵⁴R. Kavasseri and R. Nagarajan, "Evidence of crossover phenomena in wind-speed data," *IEEE Trans. Circuits Syst. I* **51**, 2255–2262 (2004).
- ⁵⁵R. Bryce and K. Sprague, "Revisiting detrended fluctuation analysis," *Sci. Rep.* **2**, 315 (2012).
- ⁵⁶O. Løvstetten, "Consistency of detrended fluctuation analysis," *Phys. Rev. E* **96**, 012141 (2017).
- ⁵⁷R. Metzler and J. Klafter, "The random walk's guide to anomalous diffusion: A fractional dynamics approach," *Phys. Rep.* **339**, 1–77 (2000).
- ⁵⁸C.-K. Peng, S. Havlin, H. Stanley, and A. Goldberger, "Quantification of scaling exponents and crossover phenomena in nonstationary heartbeat time series," *Chaos* **5**, 82–87 (1995).
- ⁵⁹Q. Ma, R. Bartsch, P. Bernaola-Galván, M. Yoneyama, and P. Ivanov, "Effect of extreme data loss on long-range correlated and anticorrelated signals quantified by detrended fluctuation analysis," *Phys. Rev. E* **81**, 031101 (2010).
- ⁶⁰K. Hu, P. Ivanov, Z. Chen, P. Carpena, and H. Stanley, "Effect of trends on detrended fluctuation analysis," *Phys. Rev. E* **64**, 011114 (2001).
- ⁶¹Z. Chen, P. Ivanov, K. Hu, and H. Stanley, "Effect of nonstationarities on detrended fluctuation analysis," *Phys. Rev. E* **65**, 041107 (2002).
- ⁶²J. Olauson, M. Bergkvist, and J. Rydén, "Simulating intra-hourly wind power fluctuations on a power system level," *Wind Energy* **20**, 973–985 (2017).
- ⁶³E. Fertig, "Simulating subhourly variability of wind power output," *Wind Energy* **22**, 1275–1287 (2019).
- ⁶⁴P.-J. Trombe, P. Pinson, and H. Madsen, "A general probabilistic forecasting framework for offshore wind power fluctuations," *Energies* **5**, 621–657 (2012).
- ⁶⁵T. Pesch, S. Schröders, H. Allelein, and J. Hake, "A new Markov-chain-related statistical approach for modelling synthetic wind power time series," *New J. Phys.* **17**, 055001 (2015).
- ⁶⁶D. Stroock, *An Introduction to Markov Processes* (Springer Science & Business Media, 2013), Vol. 230.
- ⁶⁷C. Wang, H. Zhang, W. Fan, and X. Fan, "A new wind power prediction method based on chaotic theory and Bernstein neural network," *Energy* **117**, 259–271 (2016).
- ⁶⁸H. Akçay and T. Filik, "Wind speed forecasting with missing values," in *2017 Seventh International Conference on Information Science and Technology (ICIST)* (IEEE, 2017), pp. 51–56.
- ⁶⁹D. Koutsoyiannis, "The Hurst phenomenon and fractional Gaussian noise made easy," *Hydrol. Sci. J.* **47**, 573–595 (2002).
- ⁷⁰Y. Kalmykov, W. Coffey, and S. Titov, "On the Brownian motion in a double-well potential in the overdamped limit," *Physica A* **377**, 412–420 (2007).
- ⁷¹L. Gammaitoni, P. Hänggi, P. Jung, and F. Marchesoni, "Stochastic resonance," *Rev. Mod. Phys.* **70**, 223 (1998).
- ⁷²P. Chen, P. Siano, B. Bak-Jensen, and Z. Chen, "Stochastic optimization of wind turbine power factor using stochastic model of wind power," *IEEE Trans. Sustainable Energy* **1**, 19–29 (2010).
- ⁷³L. Guan, B. Wen, Y. Zhuo, L. Wu, and B. Zhou, "Multiple wind power time series modeling method considering correlation," in *2018 International Conference on Power System Technology (POWERCON)* (IEEE, 2018), pp. 1–7.
- ⁷⁴G. Milshtein and M. Tret'yakov, "Numerical solution of differential equations with colored noise," *J. Stat. Phys.* **77**, 691–715 (1994).
- ⁷⁵A. McLeod, H. Yu, Z. Krougly *et al.*, "Algorithms for linear time series analysis: With R package," *J. Stat. Software* **23**, 1–26 (2007).
- ⁷⁶R. Friedrich, S. Siegert, J. Peinke, M. Siefert, M. Lindemann, J. Raethjen, G. Deuschl, G. Pfister *et al.*, "Extracting model equations from experimental data," *Phys. Lett. A* **271**, 217–222 (2000).
- ⁷⁷S. Siegert, R. Friedrich, and J. Peinke, "Analysis of data sets of stochastic systems," *Phys. Lett. A* **243**, 275–280 (1998).
- ⁷⁸F. Ghasemi, M. Sahimi, J. Peinke, and M. Tabar, "Analysis of non-stationary data for heart-rate fluctuations in terms of drift and diffusion coefficients," *J. Biol. Phys.* **32**, 117–128 (2006).